THE DRIVING MECHANISM OF STRONGLY DEVELOPED TAYLOR VORTEX FLOW

Thesis by

Pieter Wesseling

In Partial Fulfillment of the Requirements

For the Degree of

Doctor of Philosophy

California Institute of Technology

Pasadena, California

1967

(Submitted April 25, 1967)

ACKNOWLEDGMENTS

The author wishes to thank Professors P. A. Lagerstrom, P. G. Saffman and D. E. Coles, who suggested the subject of this thesis and gave valuable guidance. Thanks are also due to Mrs. Vivian Davies, who expertly typed the manuscript.

While engaged in the research reported in this thesis the author received financial assistance from the Ministry of Education and Sciences of the Netherlands, was holder of an International University Fellowship in Space Science, supported by the NASA and administered by the Office of Scientific Personnel of the National Academy of Sciences - National Research Council; during the year 1966-67 the author's research was sponsored by Air Force Grant No. AF-AFOSR-338-67. This support is gratefully acknowledged.

ABSTRACT

The purpose of this thesis is to explain how strongly developed Taylor vortex flow is kept in motion. On the basis of this explanation approximate torque calculations for high Taylor numbers have been made. Agreement with experiment is satisfactory. Axial symmetry is assumed throughout.

TABLE OF CONTENTS

1. Introduction

The flow between rotating concentric cylinders has attracted the attention of fluid mechanicists for a long time. One of the first papers on the subject was published in 1890 (Couette, 1890). This type of flow has several important aspects:

i) For low enough Taylor number (hereafter called T) it can be described by an exact solution of the full Navier-Stokes equations. This interested the early researchers, who wanted to check the Newtonian stress approximation in the Navier-Stokes equations against experiment.

ii) As the speed of the inner cylinder is increased the flow undergoes a sudden transition to a radically different, but again laminar flow pattern as the so-called critical Taylor number (T_c) is reached. This transition point has first been accurately predicted in a well-known paper by G. I. Taylor (1923). This was the first time a mathematical stability analysis of a flow pattern was completely in agreement with experiment. The field of hydrodynamic stability has since then been extensively developed. Both the theoretical and the experimental part of Taylor's paper were groundbreaking. In his experiment the flow pattern for $T > T_c$ was made visible; it is now often referred to as Taylor vortex flow.

iii) Above the critical Taylor number a laminar flow regime exists where the flow exhibits an interesting non-uniqueness which is of theoretical significance. For given external conditions more than one laminar flow pattern may occur (for cylinders of finite length!). Which one occurs depends on the way in which the external

conditions (speeds of cylinders) are reached. This non-uniqueness was already observed by Taylor and has recently been studied in detail by Donald Coles (Coles 1965). As T increases, an increasing number of steady (at still higher T unstable against time dependent disturbances) solutions of the Navier-Stokes equations seem to exist. A perhaps similar non-uniqueness impedes a mathematical theory of steady high Reynolds number separated flow around a finite body (Goldstein 1960 pp. 133 et seq.). The flow between rotating cylinders provides a good opportunity to study this non-uniqueness.

iv) The problem of computing the flow field at T slightly higher than T_c (non-linear stability analysis) has been undertaken by Stuart (1958) and further developed by Davey (1962). Their work compares well with experiment and is a significant contribution to nonlinear mathematics. Similar developments have taken place in the study of free thermal convection between horizontal plates (Malkus and Veronis, 1958). The interesting analogy between the flow between rotating cylinders and thermal convection between horizontal walls (noted by Rayleigh, 1916) will receive attention later in this thesis.

In view of all this work it is surprising that an explanation of the mechanism which drives the Taylor vortices is still lacking. Only in Coles' (1965) paper the present author found a first attempt to describe this mechanism. Coles' paper is devoted to other things, however, and the question receives little attention. In a recent paper Coles (1967) develops a way to make the equations dimensionless, based upon his description of the driving mechanism. As a result experimental data concerning the stability boundary collapse on certain curves. Coles'

ideas enable him to estimate the stability boundary without solving the linearized stability equations. This may be useful for flow problems for which the stability problem is difficult to solve.

Coles' description of the driving mechanism involves a complicated interaction between the equations of motion; also the mechanism which drives the flow is not immediately obvious from the equations. Coles' discussion is valid for T close to T_c. In the present thesis the case $T >> T_c$ (strongly developed Taylor vortices) is considered. It turns out that in this case the driving mechanism is simpler than in the case T close to T_c. Also, it exhibits itself more clearly in the equations.

Axial symmetry will be assumed throughout. Of course it is assumed that the flow is laminar, even though $T \to \infty$.

2. Derivation of the limiting forms of the Navier-Stokes equations as $T \to \infty$.

For an incompressible fluid the Navier-Stokes equations may be written as

$$\underline{u}^* \times \underline{\omega}^* - \nabla^*(\tfrac{1}{2}\underline{u}^* \cdot \underline{u}^* + \pi^*) - \nu \nabla^* \times \underline{\omega}^* = 0, \quad \mathrm{div}^* \underline{u}^* = 0 \qquad (2.1)$$

where π^* stands for p^*/ρ^* and asterisks indicate dimensional quantities.

The velocity components in an axial plane will be of the same order of magnitude as the forces acting in that plane. Obviously, these forces will have something to do with the difference between the centrifugal force experienced by fluid elements close to the inner and close to

the outer cylinder. Thus a typical magnitude of the acceleration perpendicular to the axis is $\left(\Omega_i^{*2} R_i^* - \Omega_u^{*2} R_u^*\right)$, hence the order of magnitude of the meridional velocity components may be expected to be $\sqrt{\left(\Omega^{*2} R_i^* - \Omega_u^{*2} R_u^*\right) d^*}$. Ω stands for angular velocity, R for radius, subscripts i and u indicate the inner and outer cylinder respectively, $d^* = R_u^* - R_i^*$.

It is convenient to put the equations in dimensionless form. As a reference velocity $\sqrt{\left(\Omega_i^{*2} R_i^* - \Omega_u^{*2} R_u^*\right) d^*}$ is chosen and as a reference length d^*. With these units (2.1) transforms into the following dimensionless equation:

$$\underline{u} \times \underline{\omega} - \nabla \left(\tfrac{1}{2} \underline{u} \cdot \underline{u} + \pi\right) - T^{-1/2} \nabla \times \underline{\omega} = 0 \qquad (2.2)$$

$$\text{div } \underline{u} = 0 \qquad (2.3)$$

Here $$T = \frac{\left(\Omega_i^{*2} R_i^* - \Omega_u^{*2} R_u^*\right) d^{*3}}{\nu^2}$$

This quantity will be called the Taylor number[/]. Here the case where T is much larger than T_c will be considered; T_c is the value of the Taylor number for which Taylor vortices just begin to appear. For large values of T the vortices are strongly developed. It is assumed that the flow is still laminar. Fig. 1 illustrates the geometry of the motion.

Since the Taylor number can be regarded as the square of a Reynolds number it seems reasonable to assume that strongly developed Taylor vortex flow will have the characteristics of a high Reynolds

---

[/] In the literature various definitions of the Taylor number have been used. The above definition seems to be the most natural one in the present context. T as defined above is the square of the ratio of centrifugal acceleration and the acceleration due to viscous forces.

number flow. It is assumed that viscous effects are only important near the boundary of each cell and not in the core of the vortices. This assumption will be correct if it leads to a self-consistent solution. It is not immediately clear that the thickness δ of this region will be of order $T^{-1/4}$ as in boundary layer theory. Again one has to make an assumption, which has to be justified by the self-consistency of the picture obtained. Perhaps the best way to arrive at the correct assumptions is by reasoning as follows. First, the inviscid region will be considered.

2.1 The inviscid region.

With the reference velocity defined above the velocity in the frictionless core will be $0(1)$. In the core the correct asymptotic expansion as $T \to \infty$ will be of the form

$$\underline{E}_u = \underline{E}_u^{(0)} + \sum_n \epsilon_n(T)\, \underline{E}_u^{(n)} \tag{2.4}$$

where $\epsilon_n(T) << 1$ and $\underline{E}_u^{(0)} = 0(1)$, $\underline{E}_u^{(n)} = 0(1)$. The ϵ_n form an asymptotic sequence as $T \to \infty$. The superscript E serves to distinguish the flow in the inviscid core (asymptotically represented by the Euler limit$^{\neq}$) from the flow in the surrounding thin viscous region (asymptotically represented by the Prandtl limit). Substituting (2.4) in (2.2) and letting $T \to \infty$ we obtain (of course) Euler's equations for $\underline{E}_u^{(0)}$

$$\left.\begin{aligned} \underline{E}_u^{(0)} \times \underline{E}_\omega^{(0)} - \nabla\left(\tfrac{1}{2}\, \underline{E}_u^{(0)} \cdot \underline{E}_u^{(0)} + E_\pi^{(0)}\right) = 0 \\ \operatorname{div} \underline{E}_u^{(0)} = 0 \end{aligned}\right\} \tag{2.5}$$

$\neq$ See Lagerstrom and Cole (1955)

In a system of polar coordinates (r, θ, z), $E_{\underline{u}}^{(0)} = (u, v, w)$, (2.5) may be written as (assuming axial symmetry)

$$u \frac{\partial u}{\partial r} + w \frac{\partial u}{\partial z} - \frac{v^2}{r} = - \frac{1}{\rho} \frac{\partial p}{\partial r}$$

$$u \frac{\partial rv}{\partial r} + w \frac{\partial rv}{\partial z} = 0$$

$$u \frac{\partial w}{\partial r} + w \frac{\partial w}{\partial z} = - \frac{1}{\rho} \frac{\partial p}{\partial z}$$

$$\frac{\partial ru}{\partial r} + \frac{\partial rw}{\partial z} = 0 \rightarrow ru = \frac{\partial \psi}{\delta z}, \quad rw = - \frac{\partial \psi}{\partial r}$$

or

$$\left. \begin{aligned} ru \frac{\partial}{\partial r} \left(\frac{\omega}{r} \right) + rw \frac{\partial}{\partial z} \left(\frac{\omega}{r} \right) &= \frac{2v}{r} \frac{\partial v}{\partial z} \\ rv &= rv(\psi) \end{aligned} \right\} \qquad (2.6)$$

where $\omega = \frac{\partial u}{\partial z} - \frac{\partial w}{\partial r}$. The boundary condition to be used with (2.6) is tangency of the flow to the cell boundary. The well-known non-uniqueness of the Euler equations under these boundary conditions is immediately obvious from (2.6). Any function $rv(\psi)$ will give a solution. For unseparated flow past a finite body in an unbounded fluid uniqueness is usually obtained by prescribing the vorticity distribution at upstream infinity. In the present case there are no streamlines which extend into a region where the vorticity is known. On the contrary, the streamlines are closed and this is precisely what enables us to formulate another condition. This condition will make the Euler solution unique apart from two constants, which have to follow from the Prandtl solution. Feynman and Lagerstrom (1956) and Batchelor (1956) studied flows with closed streamlines as the Reynolds number tends to infinity. They rediscovered results derived in Prandtl's classical boundary layer paper in 1904 (see

Prandtl 1961, p. 577). It seems appropriate to call these results Prandtl's theorem, which may be formulated as follows:

In two-dimensional flows with closed streamlines the vorticity is constant throughout the flow field as the Reynolds number tends to ∞, apart from thin boundary layers attached to the boundary of the flow field.≠

Prandtl also gave the extension of this theorem to three-dimensional axisymmetric flows: in our notation,

$$\left.\begin{aligned} rv &= \Gamma_e \\ \omega/r &= C \end{aligned}\right\} \qquad (2.7)$$

where Γ_e and C are constants.≠≠

Using (2.7), the zeroth order Euler solution can be found from

$$\left.\begin{aligned} r\,\frac{\partial}{\partial r}\left(\frac{1}{r}\,\frac{\partial \psi}{\partial r}\right) + \frac{\partial^2 \psi}{\partial z^2} &= \omega r = Cr^2 \\ rv &= \Gamma = \Gamma_e \end{aligned}\right\} \qquad (2.8)$$

The solution of (2.8) is given in the form of a Fourier-Bessel series in Appendix 3. Since Γ_e and C are unknown, the Euler solution has not yet been uniquely determined. Feynman and Lagerstrom and Batchelor realized that Γ_e and C follow from the requirement that

≠ As Feynman and Lagerstrom pointed out, the flow field may consist of several regions where the vorticity may have different magnitudes. These regions are separated from each other by thin viscous shear layers.

≠≠ The equation $\omega/r = C$ represents stretching of vortex lines. The only non-zero component of vorticity is ω. The vortex-lines are circles in planes perpendicular to the axis centered around the axis. As a fluid particle moves outward the length of the vortex-line through the particle increases proportionally to r.

there must exist a single-valued solution for the thin viscous region which surrounds the inviscid region of a cell. In order to elucidate this idea (which cannot be found in Prandtl's paper), consider the two-dimensional flow inside a circle with a velocity-distribution $u = u_w(s)$ prescribed along the circumference, where s measures distance along the circumference. According to Prandtl's theorem the vorticity is constant ($= \omega_0$, say) inside the circle. If $u_w(s)$ is not constant a boundary layer must be present along the circumference. Of course, the solution for the viscous region must be single-valued. It is shown by Feynman and Lagerstrom, that this is only possible if ω_0 has the special value $\omega_0 = \frac{2}{R}\sqrt{\overline{u_w^2}}$, where R is the radius of the circle and the bar indicates that the average is to be taken. A special case of this result is derived by Batchelor. It is very difficult to find ω_0 for contours other than a circle. In the present case the situation is even more difficult; instead of one there are two interrelated constants Γ_e and C to be determined; moreover, the viscous region contains shear layers in addition to boundary layers.

In connection with the discussion of the viscous region which will follow it is important to realize that the Euler solution has stagnation points in the corners. The Fourier-Bessel series solution of (2.8) (Appendix 3) shows stagnation points in the corners (see the plot of the radial velocity along the boundary of a cell in Fig. 7) but the Fourier-Bessel series is not accurate near the corners. In the corners of the cells ψ approximately obeys the following equation (taking a corner adjacent to the inner cylinder and letting $z = 0$ in the corner)

$$\frac{\partial^2 \psi}{\partial r^2} + \frac{\partial^2 \psi}{\partial z^2} = C R_i^2$$

with the solution, if $\psi = 0$ at $r = R_i$ and $z = 0$,

$$\psi = CR_i^2\left[\tfrac{1}{2}(r-R_i)^2+\frac{1}{\pi}(r-R_i)z\,\ell n\left\{(r-R_i)^2+ z^2\right\} - \frac{1}{\pi}\left\{(r-R_i)^2-z^2\right\}\tan^{-1}\frac{r-R_i}{z}\right] \quad (2.9)$$

Because the boundary conditions for (2.8) have not been prescribed on a closed boundary the solution (2.9) is not unique; harmonic terms like rz may be added. But in the corner these will be small compared to the logarithmic term. From (2.9) follows that $\frac{\partial\psi}{\partial r}$ and $\frac{\partial\psi}{\partial z}$ are zero in the corners. Hence the Euler solution has stagnation points in the corners. This deduction has far reaching consequences for the viscous region, which will now be considered.

2.2 The viscous region

Consider the boundary layer AB (Fig. 1) attached to the inner cylinder, excluding the corner regions.

The assumption that the viscous region is thin implies that the "thickness" of the corner region, though possibly of a different order of magnitude than the thickness of the rest of the viscous region, is negligible compared to the overall dimensions of the cell. It also follows that the pressure in the viscous region is equal to the pressure at the edge of the viscous region, which can be found from the Euler solution. Therefore the pressure in A and B equals the pressure of the Euler solution in the corners. Since these are stagnation points for the Euler solution, $\pi_A = \pi_B$. Between A and B, $\pi < \pi_A$. In order to match with the Euler solution the velocity in AB must be 0(1). There may be a velocity overshoot in AB (this will turn out to be the case) but since there are no forces acting on the flow greater than 0(1) the overshoot can never be greater than 0(1). In AB the frictional term in the Navier-Stokes equations is approximately

$T^{-1/2} \frac{\partial^2 u}{\partial r^2}$ where $u = 0(1)$. Requiring this term to be $0(1)$ as $T \to \infty$ (Goldstein, 1960) gives for the thickness of AB: $\delta = O(T^{-1/4})$. Hence the flow in AB is described by Prandtl's boundary layer equations. The same reasoning applies to the other parts of the viscous region, the corner regions excluded. The equations for the viscous region can be found by making the boundary layer simplifications in the Navier-Stokes equations. If there is no velocity overshoot in AB orthodox boundary layer theory applies. The boundary layer AB begins with a stagnation point in A, goes through a region of pressure decrease, reaches the pressure minimum midway between A and B, and separates shortly after this pressure minimum has been passed, at a considerable distance before B. The separation bubble which would result would be large enough to be observed by experimenters. It would have manifested itself in the detailed measurements of the flow recently taken by Snyder and Lambert (1966). Since this is not the case the picture just drawn is almost certainly wrong. The only way to maintain the assumption that the cell has an inviscid core surrounded by a thin viscous region is by assuming that the boundary layer begins at A with a velocity overshoot large enough to prevent separation between A and B; this velocity overshoot must therefore be at least $0(1)$. Since no forces greater than $0(1)$ are present, the velocity overshoot at A cannot be greater than $0(1)$. Thus the typical velocity in the corner regions is appreciably greater than zero, although the outer velocity is zero in the corners.

The viscous term in the Navier-Stokes equation is approximately in the corners:

$$T^{-1/4}\left(\frac{\partial^2 u}{\partial r^2}+\frac{\partial^2 u}{\partial z^2}\right) \qquad \text{(r-direction)}$$

$$T^{-1/4}\left(\frac{\partial^2 w}{\partial r^2}+\frac{\partial^2 w}{\partial z^2}\right) \qquad \text{(z-direction)}$$

According to the reasoning given above u, w are $0(1)$ in the corners. Requiring again that the dissipation be $0(1)$ as $T \to \infty$ gives for the thickness of the corner regions (see Fig. 3).

$$\delta = O(T^{-1/4})$$

These results can be summarized as follows: away from the corners, Prandtl's boundary layer approximations are valid. The thickness of the corner regions is of the same order as the boundary layer thickness, which is in terms of the Taylor number $\delta = O(T^{-1/4})$.

It is convenient to describe the viscous region with the coordinate system (s,n) depicted in Fig. 2. Lines $n = \text{constant}$ are parallel to the cell boundary, perpendicular to these are lines $s = \text{constant}$. Outside the corner regions every point in the viscous region is uniquely defined by one value of s and n. s runs from s_0 to s_4. Application of the boundary layer simplifications in the Navier-Stokes equations results in the following equations for the viscous region, the corners excluded:

(M.S.)

$$U\frac{\partial U}{\partial s}+W\frac{\partial U}{\partial n}=U_e\frac{dU_e}{ds}+\frac{\Gamma^2-\Gamma_e^2}{r^3}\cdot\frac{\partial r}{\partial s}+T^{-1/2}\frac{\partial^2 U}{\partial n^2} \qquad (2.10a)$$

$$U\frac{\partial \Gamma}{\partial s}+W\frac{\partial \Gamma}{\partial n}=T^{-1/2}\frac{\partial^2 \Gamma}{\delta n^2} \qquad (2.10b)$$

$$\frac{\partial rU}{\partial s}+\frac{\partial rW}{\partial n}=0 \qquad (2.10c)$$

where U, W are velocity components in the s and n directions respectively, $\Gamma = rv$ and U_e is the velocity at the boundary of the inviscid core as given by the Euler solution. Equations (2.7), (2.8) and (2.10) are the limiting forms of the Navier-Stokes equations as $T \to \infty$.

The constants Γ_e and C should follow from the requirement that the solution of (2.10) be periodic in s.

3. The physical mechanism by which the Taylor vortices are driven

From equations (2.10) the driving mechanism of strongly developed Taylor-vortex flow is immediately apparent. For strongly developed vortices the inner cylinder has to rotate much faster than the outer one, or more precisely

$$\Gamma_i >> \Gamma_u$$

where subscripts i and u indicate respectively the inner and outer cylinder. Γ_e will have an intermediate value. In the subregion AB (see Fig. 1) the inner cylinder imparts angular momentum to the fluid in the viscous region. Close to B we will have $\Gamma_i > \Gamma > \Gamma_e$. According to (2.10b) the angular momentum is then convected downstream while it diffuses into the inviscid core. In BC $\Gamma > \Gamma_e$ everywhere. The term labeled (M.S.) in (2.10a) is therefore positive everywhere in BC; it is the mathematical representation of a momentum source which accelerates the fluid outward. Apart from non-linear interactions the pressure term does not give a net acceleration since $\pi_B = \pi_C$.

Therefore, under the action of the momentum source described by (M.S.) the fluid in the thin viscous shear layer BC is accelerated outward and impinges jet-like on the outer cylinder. This jet then spreads out on the outer cylinder as a boundary-layer with a velocity overshoot (a wall-jet). That a velocity overshoot must exist in order to prevent boundary layer separation between C and D was shown in section 2 of this thesis.

In a discussion with the author, Professor Saffman suggested that it seems likely that the possibility of boundary layer separation between A and B or C and D accounts for the phenomenon of state transition, i.e. changes in the cell pattern. Presumably, if the speed of the cylinders is varied in such a way that the boundary layer separates between A and B or C and D a state transition occurs.

In the subregion CD angular momentum is lost to the slowly rotating outer cylinder; near D, $\Gamma_e > \Gamma > \Gamma_u$. Again, in DA the term (M.S.) is positive, it represents a momentum source which accelerates the fluid in the thin shear layer DA inward. (Note that here s is counted positive inward, so that $\partial r/\partial s = -1$). At A, the fluid impinges jet-like on the inner cylinder so that the boundary layer AB has at A a velocity overshoot large enough to prevent separation between A and B. It is now clear why frictional forces do not inhibit Taylor vortex motion; they are balanced by the momentum source.

The momentum source (M.S.) gives rise to velocity components in an axial plane with magnitude of order $\left\{ d \left(\frac{\Gamma_i^2}{R_i^3} - \frac{\Gamma_u^2}{R_u^3} \right) \right\}^{1/2}$.

The reference velocity has been chosen such that this quantity is 1. It is interesting to note that the secondary motion (the motion in an axial plane) is of the same order of magnitude as the "primary" motion (the motion in the circumferential direction).

A physical description of the momentum source can be given as follows. The forces working on a rotating fluid are pressure forces, centrifugal forces and viscous forces. (If the angular momentum $\Gamma = rv$ of a fluid particle is taken as dependent variable instead of the angular velocity v Coriolis terms do not appear). The pressure gradient in the viscous shear layer BC is the same as in the adjacent part of the inviscid core. The angular momentum in BC (where the fluid has passed closely to the fast rotating inner cylinder) is considerably larger than the angular momentum in the inviscid core. Therefore the outward acceleration in the shear layer is larger than in the inviscid core. Therefore $U > U_e$ in BC; as the shear layer moves outward this jet-like velocity overshoot grows. The acceleration of the shear layer flow (U) relative to the core flow (U_e) finds its mathematical expression in the term (M.S.) in (2.10a).

The jet-like behavior of the outward moving shear layer has been observed experimentally by Snyder and Lambert. However they observed a slow inflow. Approximate calculations to be given later in this thesis do indeed indicate that the speed in the inward moving shear layer is appreciably less than the speed in the outward moving shear layer. If Snyder's and Lambert's experiments were repeated at a higher Taylor number (assuming this is possible with turbulence being absent) the jet-like behavior of the inward moving shear layers would

presumably become apparent.

From (2.10b) (as well as from the full Navier-Stokes equations) it is clear that Γ is convected and diffused just like heat. Equations (2.10a) and (2.10b) are reminiscent of the Boussinesq equations for a viscous fluid with temperature differences and buoyancy forces. A difference is that the term (M.S.) is quadratic in Γ, whereas the buoyancy force is linear in the temperature. The close analogy between rotating fluid motions and fluid motion with buoyancy forces due to temperature differences was used with great advantage by Lord Rayleigh; he derived his well-known stability criterion for inviscid rotating flows in analogy with the stability of a liquid of variable density in a gravitational field (Rayleigh, 1916).

Approximate calculations of the Nusselt number at high Rayleigh numbers for a horizontal layer of fluid heated from below can be made in the same fashion as the following approximate torque calculations.

4. Approximate torque calculation.

A solution of the equation for the inviscid region (2.8) is easily calculated, for example in the form of a Fourier-Bessel series. (Appendix 3). Equations (2.10) however are difficult to solve. They resemble the usual boundary layer equations closely but are even more difficult. The velocity overshoot gives an added complication. Moreover, at no value of s a velocity profile is known in advance, as is usually the case in boundary layer problems. Also, the boundary

conditions at $n = \infty$ are not known completely but involve constants Γ_e and C. These constants have to be determined from the condition that the solution for u and Γ must be periodic in s. The flow in the corners is governed by the full Navier-Stokes equations.

Due to these complications even the approximate methods which have been developed over the years for solving the boundary layer equations require extensive numerical work in addition to crude approximations.

Because of these difficulties it is perhaps useful to make a rough calculation of the most important quantity, the torque, without aiming for numerical accuracy. Such a calculation is presented below. The resulting torque predictions are almost 30 % higher than experimental results.

4.1 The radial shear layers.

An approximate solution of the radial shear layers BC and DA is sought by assuming certain velocity profiles which do not satisfy the exact equations but integrated forms of the equations. This is the underlying idea of the well-known Karman-Pohlhausen technique.

The symmetry of the cell-structure requires that the velocity profiles in the shear layers be even in n. The following profiles are chosen:

$$U(s,n) = U_e(s) + S(s)e^{-\eta^2}$$

$$\Gamma(s,n) = \Gamma_e + \theta(s)e^{-\eta^2} \qquad (4.1.1)$$

$$\eta = \frac{n}{\delta(s)}$$

where $\delta(s)$ is still to be determined. These profiles satisfy the boundary conditions at $n = \infty$.

Three equations are needed in order to determine the three unknown functions $S(s)$, $\theta(s)$, and $\delta(s)$. It is convenient to select:

i) The meridional momentum-integral equation.

ii) The angular momentum-integral equation.

iii) The equation for the angular momentum taken at $n = 0$.

In the free shear layers these equations are respectively

$$\frac{d}{ds}\left\{\int_0^\infty rU(U-U_e)dn\right\} + \frac{dU_e}{ds}\int_0^\infty r(U-U_e)dn = \frac{1}{r^2}\frac{dr}{ds}\int_0^\infty (\Gamma^2-\Gamma_e^2)dn \qquad (4.1.2)$$

$$\frac{d}{ds}\left\{\int_0^\infty rU(\Gamma-\Gamma_e)dn\right\} = 0 \qquad (4.1.3)$$

$$U(s,0)\ \frac{\partial\Gamma}{\partial s}\bigg|_{n=0} = T^{-1/4}\ \frac{\partial^2\Gamma}{\partial n^2}\bigg|_{n=0} \qquad (4.1.4)$$

The derivation of (4.1.2) and (4.1.3) is given in Appendix 2.

Substitution of (4.1.1) gives

$$\frac{d}{ds}\left\{r\,\delta S(S+U_e\sqrt{2})\right\} + \frac{dU_e}{ds} rS\,\delta\sqrt{2} = \frac{1}{r^2}\frac{dr}{ds}\,\delta\theta(\theta+\Gamma_e\sqrt{2}) \qquad (4.1.5)$$

$$\frac{d}{ds}\left\{r\,\delta\theta\,(S+U_e\sqrt{2})\right\} = 0 \qquad (4.1.6)$$

$$(U_e+S)\frac{d\theta}{ds} = -2T^{-1/4}\frac{\theta}{\delta^2} \qquad (4.1.7)$$

From (4.1.6) follows

$$r\,\delta\theta\,(S+U_e\sqrt{2}) = \text{constant} = \sqrt{\frac{8}{\pi}}\,M_j \qquad (4.1.8)$$

where $j=1$ in the outward moving shear layer BC and $j=3$ in the inward moving shear layer DA. Equation (4.1.8) says that the flux

of angular momentum

$$M = 2\pi r \int_0^\infty U(\Gamma-\Gamma_e)\, dn$$

is constant in the shear layers, in accordance with the close analogy between angular momentum flux and heat flux which was noted before.

With (4.1.8) δ is eliminated from (4.1.5) and (4.1.6):

$$\frac{d}{ds}\left(\frac{S}{\theta}\right) + \frac{dU_e}{ds}\,\frac{S\sqrt{2}}{\theta\left(S+U_e\sqrt{2}\right)} = \frac{1}{r^3}\frac{dr}{ds}\,\frac{\theta+\Gamma_e\sqrt{8}}{S+U_e\sqrt{2}} \qquad (4.1.9)$$

$$(U_e + S)\frac{d\theta}{ds} = -\frac{2}{T^{1/2}}\,\frac{\pi}{8}\,\frac{r^2\theta^3}{M_j^2}\left(S + U_e\sqrt{2}\right)^2 \qquad (4.1.10)$$

Solving these two simultaneous non-linear ordinary differential equations is still difficult. The problem is further simplified by assuming that θ retains the value it has at the beginning of the free shear layer throughout the whole shear layer. That is

$$\theta = \theta_{i,u} = \begin{cases} \theta_i & \text{for the outward moving shear layer} \\ \theta_u & \text{for the inward moving shear layer} \end{cases} \qquad (4.1.11)$$

For the outward moving shear layer this is an overestimation of θ, which according to (4.1.9) results in an overestimation of S. Then according to (4.1.8) δ is underestimated. Therefore, in quantities like the flux of meridional kinetic energy $\left(\int_0^\infty U^3\, dn\right)$ and meridional mass flux $\left(\int_0^\infty U\, dn\right)$ which involve the products $V^3\delta$ and $V\delta$ the error in V and δ have opposite influence, which is fortunate.

With $\theta = \theta_{i,u}$ (4.1.9) can be written as

$$\left(S + U_e\sqrt{2}\right)\frac{dS}{ds} + S\,\frac{dU}{ds}e\,\sqrt{2} = \frac{1}{r^3}\,\frac{dr}{ds}\,\theta_{i,u}\left(\theta_{i,u} + \Gamma_e\sqrt{8}\right)$$

or

$$\frac{d}{dr}\left(\tfrac{1}{2}S^2 + U_e\, S\sqrt{2}\right) = \frac{1}{r^3}\,\theta_{i,u}\left(\theta_{i,u} + \Gamma_e\sqrt{\delta}\right)$$

Hence

$$\left(S^2 + U_e S\sqrt{8}\right)\Big|_{r=R_u} = \left(S^2 + U_e S\sqrt{8}\right)\Big|_{r=R_i} + \theta_{i,u}\left(\theta_{i,u} + \Gamma_e\sqrt{8}\right)\left(1/R_i^2 - 1/R_u^2\right)$$

Since $U_e = 0$ in the corners

$$\begin{aligned} S_2^2 &= S_1^2 + \theta_i\left(\theta_i + \Gamma_e\sqrt{8}\right)\left(1/R_i^2 - 1/R_u^2\right) \\ S_4^2 &= S_3^2 - \theta_u\left(\theta_u + \Gamma_e\sqrt{8}\right)\left(1/R_i^2 - 1/R_u^2\right) \end{aligned} \qquad (4.1.12)$$

Here subscripts 1, 2, 3, 4 indicate the various corners of the cell according to Fig. 2.

Because of the accelerating action of the centrifugal forces in the free shear layers the meridional speed, momentum and kinetic energy are much larger at the points of impingement (4 and 2) than at the points of separation (1 and 3). Therefore in (4.1.12) S_1 and S_3 are neglected. This simplifies the problem considerably because the algebra required for the matching of the solutions for the shear layers and the wall-jets becomes much less involved.

Thus (4.1.2) becomes

$$\begin{aligned} S_2^2 &= \theta_i\left(\theta_i + \Gamma_e\sqrt{8}\right)\left(1/R_i^2 - 1/R_u^2\right) \\ S_4^2 &= -\theta_u\left(\theta_u + \Gamma_e\sqrt{8}\right)\left(1/R_i^2 - 1/R_u^2\right) \end{aligned} \qquad (4.1.13)$$

(4.1.8) gives

$$\delta_2 = \sqrt{\frac{8}{\pi}}\,\frac{M_1}{R_u\theta_i S_2} \qquad (4.1.14a)$$

$$\delta_4 = \sqrt{\frac{8}{\pi}}\ \frac{M_3}{R_i \theta_u S_4} \tag{4.1.14b}$$

The meridional kinetic energy flux $E = 2\pi r \int_0^\infty U^3\, dn$ at the points of impingement is:

$$\begin{aligned} E_2 &= \pi \sqrt{\frac{8}{3}}\ M_1 \left(\theta_i + \Gamma_e \sqrt{8}\right)\left(1/R_i^2 - 1/R_u^2\right) \\ E_4 &= -\pi \sqrt{\frac{8}{3}}\ M_3 \left(\theta_u + \Gamma_e \sqrt{8}\right)\left(1/R_i^2 - 1/R_u^2\right) \end{aligned} \tag{4.1.15}$$

The meridional mass flux $Q = 2\pi r \int_0^\infty U\, dn$ at the points of impingement is:

$$\begin{aligned} Q_2 &= \pi \sqrt{8}\ \frac{M_1}{\theta_i} \\ Q_4 &= \pi \sqrt{8}\ \frac{M_3}{\theta_u} \end{aligned} \tag{4.1.16}$$

This completes the approximate calculation of the shear layers.

4.2 The corner regions.

The flow in the corner regions is governed by the full Navier-Stokes equations, also in the limit $T \to \infty$. The exact stagnation point similarity solution of the Navier-Stokes equations is of no use here, because it cannot simulate the very important jet-like behavior of the impinging shear layer and the velocity overshoot in the boundary layer at the cylinder wall. Also, the exact solution has zero vorticity at infinity. The solution to be used for the corner regions must necessarily be approximate. Such a solution based on qualitative considerations may be obtained as follows.

In section 2 it was shown that the thickness of the corner

regions is $\delta = 0(T^{-1/4})$. The energy dissipation in the corners is $0(1)$ as $T \to \infty$, as in the rest of the viscous region. The ratio of the dissipation in the corner regions and the dissipation taking place in the wall-jets and shear layers equal therefore the ratio of the volumes of these two regions: $\frac{2\pi r \delta^2}{2\pi r \delta d} = \frac{\delta}{d}$. It follows that the energy dissipated in the corner regions is much less than the energy dissipated in the rest of the viscous region. Therefore it seems a good approximation to neglect the energy dissipation in the corner regions. The meridional kinetic energy flux E is assumed to be constant in the corner regions.

Assuming a continuous flow field it follows also from the small dimensions of the corner regions that the mass flux in the viscous region changes little in the corners. The meridional mass flux Q is also assumed constant in the corner regions.

These two assumptions will suffice to obtain an approximate solution for the viscous region.

4.3 The wall-jets.

The wall-jets constitute the most complicated part of the viscous region.

Themost straightforward way to obtain an approximate solution for the wall-jets would be to proceed along the lines of the Karman Pohlhausen technique, as was done for the shear layers. The velocity profile chosen should be of the type given in Fig. 3 and would therefore be complicated. In addition to the boundary layer thickness $\delta(s)$ functions describing magnitude and distance from the wall of the maximum velocity overshoot should be introduced. Because the pressure-gradient $-U_e \frac{dU_e}{ds}$ is not zero or constant the resulting simultaneous

ordinary differential equations would have to be solved numerically, or additional approximations would have to be made.

For simplicity's sake we put $U_e = 0$ in equations (2.10) and let $u \to 0$ as $n \to \infty$. Then (2.10) has an exact similarity solution which satisfies the requirement of having a velocity overshoot and can be easily matched with the impinging shear layer. The similarity solution for (2.10a) with $U_e = 0$ (remember that $\frac{\partial r}{\partial s} = 0$ in the wall-jets) and (2.10c) has been studied and graphically represented by Glauert (1956) who called the type of flow associated with it a wall-jet. This similarity solution will here be extended to include (2.10b). In fact, in so doing an exact solution of the boundary layer equations with heat transfer will be obtained, for Glauert's wall-jet similarity case.

The approximate equations which will be solved exactly to obtain an approximate solution for the wall-jets are

$$U \frac{\partial U}{\partial s} + W \frac{\partial U}{\partial n} = T^{-\frac{1}{2}} \frac{\partial^2 U}{\partial n^2} \tag{4.3.1}$$

$$U \frac{\partial \Gamma}{\partial s} + W \frac{\partial \Gamma}{\partial n} = T^{-\frac{1}{2}} \frac{\partial^2 \Gamma}{\partial n^2} \tag{4.3.2}$$

$$\frac{\partial rU}{\partial s} + \frac{\partial rW}{\partial n} = 0 \tag{4.3.3}$$

The boundary conditions to be used are

$$U(s,0) = U(s,\infty) = 0 \tag{4.3.4}$$

$$\Gamma(s,0) = \Gamma_{i,u}\,, \quad \Gamma(s,\infty) = \Gamma_e \tag{4.3.5}$$

where

$$\Gamma_{i,u} = \begin{cases} \Gamma_i & \text{at the inner cylinder} \\ \Gamma_u & \text{at the outer cylinder} \end{cases}$$

(4.3.4) is not exact, (4.3.5) is.

For a unique solution an initial condition at $s = 0$ is necessary in addition to (4.3.4), (4.3.5). This condition is that the wall-jet must be a continuation of the flow in the upstream corner. This condition will be approximately satisfied by requiring the mass and kinetic energy fluxes Q and E at the beginning of the wall-jet to be equal to Q and E in the adjacent corner.

Using Glauert's work the following solution of (4.3.1) and (4.3.3) can be written down:

$$\left.\begin{aligned} \psi &= \left\{ \frac{40F_{i,u}\left(s-\sigma_{i,u}\right)}{T^{1/2}} \right\}^{1/4} f(\eta) \\ U &= \left\{ \frac{5F_{i,u}\,T^{1/2}}{2\left(s-\sigma_{i,u}\right)} \right\}^{1/2} f'(\eta) \\ \eta &= \left\{ \frac{5F_{i,u}\,T^{3/2}}{32\left(s-\sigma_{i,u}\right)^3} \right\}^{1/4} n \end{aligned}\right\} \qquad (4.3.6)$$

Here $f(\eta)$ is the solution of

$$\left.\begin{aligned} f''' + ff'' + 2f'^2 &= 0 \\ f(0) = f(\infty) &= 0 \end{aligned}\right\} \qquad (4.3.7)$$

f and f' are given by Glauert in graphical form.

$$\sigma_{i,u} = \begin{cases} \sigma_i & \text{at the inner cylinder} \\ \sigma_u & \text{at the outer cylinder} \end{cases}$$

$s = \sigma_{i,u}$ is what will be called the singular point of the similarity solution. It will be determined by matching the wall-jets with the impinging shear layers. It is not assumed that the singular points coincide with the points of impingement, as in Glauert's work.

The constant $F_{i,u}$ is the scale of the similarity profile. It has a rather obscure physical interpretation: from (4.3.1), (4.3.3) and (4.3.4) can be deduced in a straightforward way (see Glauert, (1956)) that

$$\int_0^\infty U \left\{ \int_n^\infty U^2 \, dn \right\} dn = \text{constant} = F_{i,u} \tag{4.3.8}$$

$F_{i,u}$ might be called the "exterior flux of momentum flux". As Glauert observes, this is hardly a familiar concept. (4.3.8) holds for similar as well as for non-similar solutions.

With (4.3.6) the meridional mass flux Q and kinetic energy flux E is found to be

$$Q = 4\pi \left(\frac{5}{2}\right)^{1/4} R_{i,u} F_{i,u}^{1/4} \frac{(s-\sigma_{i,u})^{1/4}}{T^{1/8}} \tag{4.3.9}$$

$$E = 10\pi \left(\frac{5}{2}\right)^{1/4} e_1 R_{i,u} \frac{F_{i,u}^{5/4} T^{3/8}}{(s-\sigma_{i,u})^{3/4}} \tag{4.3.10}$$

where $e_1 = \int_0^\infty f'^3(\eta) \, d\eta = \frac{8}{140}$ (using 4.3.7).

From (4.3.9) and (4.3.10) follows

$$F_{i,u} = \frac{1}{40\pi^2\sqrt{e_i}} \frac{\sqrt{EQ^3}}{R_{i,u}^2} \tag{4.3.11}$$

$$s-\sigma_{i,u} = \frac{\sqrt{e_1}}{16\pi^2} \frac{T^{1/2}}{R_{i,u}^2} \sqrt{\frac{Q^5}{E}} \tag{4.3.12}$$

From (4.3.11) follows that for the Glauert similarity profile $E\,Q^3$ is constant in the wall-jets. Close to the upstream corner region the velocity profile may differ from the similarity profile. But a profile

$$U = V(s)\,\frac{n}{\delta(s)}\,\exp\left\{-\,\frac{n^2}{\delta^2(s)}\right\}$$

(this profile has a velocity overshoot) also has $E\,Q^3 = \text{constant}$ if (4.3.8) is satisfied, for otherwise arbitrary $V(s)$ and $\delta(s)$. Hence the assumption that EQ^3 does not vary in the wall-jet seems a reasonable approximation. Thus

$$EQ^3 = \text{constant} = E_\ell Q_\ell^3 \tag{4.3.13}$$

where E_ℓ and Q_ℓ are the impinging meridional kinetic energy and mass fluxes. At the inner cylinder $\ell = 4$, at the outer $\ell = 2$. Since it has been assumed that E and Q do not vary in the corner regions E_ℓ and Q_ℓ are known from the approximate shear layer solution. Therefore the scale of the similarity solution is known:

$$F_{i,u} = \frac{1}{40\pi^2\sqrt{e_1}}\;\frac{\sqrt{EQ^3}}{R_{i,u}^2} \tag{4.3.14}$$

The wall-jet is further matched with the impinging shear layer by requiring that $\frac{Q^5}{E}$ at the beginning of the wall-jet equals $\frac{Q^5}{E}$ in the impinging shear layer. With (4.3.12) this determines the location of the singular point $\sigma_{i,u}$ of the wall-jet:

$$s_\ell - \sigma_{i,u} = \frac{\sqrt{e_1}}{16\pi^2}\;\frac{T^{1/2}}{R_{i,u}^2}\;\sqrt{\frac{Q_\ell^5}{E_\ell}} \tag{4.3.15}$$

Of course the singular point does not occur in the real flow; $s = \sigma_{i,u}$ is the "virtual" starting point of the wall-jet.

With $F_{i,u}$ and $\sigma_{i,u}$ determined in this way the meridional mass and kinetic energy fluxes Q and E are continuous through the regions where the shear layers impinge on the cylinder walls.

The appropriate solution of (4.3.1) and (4.3.3) with boundary conditions (4.3.4) is now fully known; equation (4.3.2) with boundary conditions (4.3.5) remains to be solved. Fortunately several similarity solutions exist which make an exact solution possible. By separation of variables the following solutions of (4.3.2) are easily derived:

$$\Gamma = C \int_0^{\eta} \exp\left\{-\int_0^{\eta_1} f(\eta_2)\, d\eta_2\right\} d\eta,$$

with f given by (4.3.7) and

$$\Gamma = Bu$$

with u given by (4.3.6). The following solution satisfies the boundary conditions (4.3.5):

$$\Gamma - \Gamma_e = B_{i,u} + \left(\Gamma_{i,u} - \Gamma_e\right)\left[1 - \frac{1}{e_2}\int_0^{\eta} \exp\left\{-\int_0^{\eta_1} f(\eta_2) d\eta_2\right\} d\eta_1\right] \qquad (4.3.16)$$

with $e_2 = \int_0^{\infty} \exp\left\{-\int_0^{\eta_1} f(\eta_2) d\eta_2\right\} d\eta_1 = 3$. The constant $B_{i,u}$ is chosen such that the meridional flux of angular momentum

$$M = 2\pi R_{i,u} \int_0^{\infty} U(\Gamma - \Gamma_e)\, d\eta$$

at the beginning of the wall-jet equals the angular momentum flux in the impinging shear layer. With $(\Gamma - \Gamma_e)$ given by (4.3.16) it follows that

$$M = 2\pi R_{i,u}\left[B_{i,u}\frac{2}{9}\left\{\frac{250F_{i,u}^3T^{1/2}}{s_\ell-\sigma_{i,u}}\right\}^{1/4}\left(\frac{s_\ell-\sigma_{i,u}}{s-\sigma_{i,u}}\right)^{1/4}+\right.$$

$$\left.+\frac{1}{3}\left(\Gamma_{i,u}-\Gamma_e\right)\left\{\frac{40F_{i,u}\left(s_\ell-\sigma_{i,i}\right)}{T^{1/2}}\right\}^{1/4}\left(\frac{s-\sigma_{i,u}}{s_\ell-\sigma_{i,u}}\right)^{1/4}\right.$$

By requiring at $s = s_\ell$, $M = M_\ell$ = meridional angular momentum flux in shear layers at points if impingement ($\ell = 2$ at the outer cylinder, $\ell = 4$ at the inner cylinder) the constant $B_{i,u}$ may be determined. One obtains for M:

$$M = M_\ell\left(\frac{s_\ell-\sigma_{i,u}}{s-\sigma_{i,u}}\right)^{1/4}+$$

$$+\frac{2\pi}{3}R_{i,u}(\Gamma_{i,u}-\Gamma_e)\left\{\frac{40F_{i,u}\left(s_\ell-\sigma_{i,u}\right)}{T^{1/2}}\right\}^{1/4}\left\{\left(\frac{s-\sigma_{i,u}}{s_\ell-\sigma_{i,u}}\right)^{1/4}-\left(\frac{s_\ell-\sigma_{i,u}}{s-\sigma_{i,u}}\right)^{1/4}\right\} \qquad (4.3.17)$$

From (4.3.11), (4.3.12), (4.1.15) and (4.1.16) follows, remembering that $M_1 = M_2$, $M_3 = M_4$:

$$\left\{\frac{40F_{i,u}\left(s_\ell-\sigma_{i,u}\right)}{T^{1/2}}\right\}^{1/4} = \sqrt{2}\,\frac{M_\ell}{R_{i,u}\,\theta_\ell} \qquad (4.3.18)$$

It is also assumed that M is continuous through those corner regions where the flow separates from the walls. Substitution of (4.3.18) in (4.3.17) then gives the following equations:

$$M_1 = M_3\left\{\left(\frac{s_0-\sigma_i}{s_0-\sigma_i+h}\right)^{1/4}\left(1+\frac{\pi\sqrt{8}}{3}\frac{\Gamma_i-\Gamma_e}{\Gamma_e-\Gamma_u}\right)-\frac{\pi\sqrt{8}}{3}\frac{\Gamma_i-\Gamma_e}{\Gamma_e-\Gamma_u}\left(\frac{s_0-\sigma_i+h}{s_0-\sigma_i}\right)^{1/4}\right\} \qquad (4.3.19)$$

$$M_3 = M_1\left\{\left(\frac{s_2-\sigma_u}{s_2-\sigma_u+h}\right)^{1/4}\left(1+\frac{\pi\sqrt{8}}{e_2}\frac{\Gamma_e-\Gamma_u}{\Gamma_i-\Gamma_e}\right)-\frac{\pi\sqrt{8}}{3}\frac{\Gamma_e-\Gamma_u}{\Gamma_i-\Gamma_e}\left(\frac{s_2-\sigma_u+h}{s_0-\sigma_i}\right)^{1/4}\right\} \qquad (4.3.20)$$

where h is the height of one cell (see Fig. 1).

The approximate solution of M as derived in this way is continuous and single-valued. A consequence is that the torques on the cylinders are equal and opposite, as they should be. (The outer cylinder takes as much angular momentum out of the flow as the inner cylinder puts in).

With (4.3.12), (4.1.15) and (4.1.16):

$$s_0 - \sigma_u = \frac{3^{1/4}}{2} \sqrt{e_1}\, \frac{T^{1/2}}{R_i^2}\, M_3^2\, \theta_3^{-2} \left\{ -\theta_u \left(\theta_u + \Gamma_e \sqrt{8} \right) \right\}^{-1/2} \left(1/R_i^2 - 1/R_u^2 \right)^{-1/2} \qquad (4.3.21)$$

$$s_2 - \sigma_u = \frac{3^{1/4}}{2} \sqrt{e_1}\, \frac{T^{1/2}}{R_u^2}\, M_1^2\, \theta_i^{-2} \left\{ \theta_i \left(\theta_i + \Gamma_e \sqrt{8} \right) \right\}^{-1/2} \left(1/R_i^2 - 1/R_u^2 \right)^{-1/2} \qquad (4.3.22)$$

The four equations (4.3.19) - (4.3.22) contain five unknowns: M_1, M_2, Γ_e, σ_i and σ_u. An additional equation is needed.

Single-valuedness of M is a necessary but not sufficient condition for single-valuedness of Γ. Another necessary condition for single-valuedness of Γ can be derived as follows. The equation for Γ (2.10b) can be written as

$$\frac{\partial \Gamma}{\partial s} + \frac{W}{U} \frac{\partial \Gamma}{\partial n} = T^{-1/2} \frac{I}{U} \frac{\partial^2 \Gamma}{\partial n^2}$$

Transformation from independent variables (s,n) to independent variables (t,x) where $t = s$ and x is the streamfunction (the von Mises transformation) gives

$$\frac{\partial \Gamma}{\partial t} = T^{-1/2} \frac{\partial}{\partial x} \left(U \frac{\partial \Gamma}{\partial x} \right)$$

For single-valuedness of Γ it is necessary and sufficient that

$$\oint \frac{\partial \Gamma}{\partial t}\, dt = 0 \quad \text{along each streamline, or}$$

$$\oint \frac{\partial}{\partial x}\left(U \frac{\partial \Gamma}{\partial x}\right) dt = 0 \quad \text{along each streamline.}$$

At the streamline $x = 0$: $\frac{\partial}{\partial x} = \frac{1}{U}\frac{\partial}{\partial n}$, $dt = ds$.

Hence

$$\oint \left\{ \frac{1}{U} \frac{\partial^2 \Gamma}{\partial n^2} \right\}\Big|_{n=0} ds = 0 \tag{4.3.23}$$

Equation (4.3.23) is a necessary condition for a single-valued solution for Γ. Substitution of the approximate shear-layer solution in (4.3.23) gives

$$\frac{\theta_i^3}{M_1^2} \sqrt{\theta_i(\theta_i+\Gamma_e\sqrt{8})} + \frac{\theta_u^3}{M_3^2} \sqrt{-\theta_u(\theta_u+\Gamma_e\sqrt{8}} = -$$

or

$$\frac{1}{M_3^2} = \frac{1}{M_1^2}\kappa^3 \sqrt{\kappa \frac{\theta_i+\Gamma_e\sqrt{8}}{\theta_u+\Gamma_e\sqrt{8}}} \tag{4.3.24}$$

where $\kappa = -\frac{\theta_i}{\theta_u} = \frac{\Gamma_i-\Gamma_e}{\Gamma_e-\Gamma_u}$. Note that $\theta_u = \Gamma_u - \Gamma_e$ is negative. We now have obtained five simultaneous non-linear algebraic equations (4.3.19)-(4.3.22) and (4.3.24) for the five unknowns $M_1, M_2, \Gamma_e, \sigma_i$, and σ_u. These equations can be solved as follows.

Substitution of (4.3.24) in (4.3.21) and (4.3.22) gives

$$s_2 - \sigma_u = \alpha(s_0 - \sigma_i) \quad \text{with} \quad \alpha = \frac{R_i^2}{R_u^2}\kappa^3 \tag{4.3.25}$$

Substitution of (4.3.24) in (4.3.19) and (4.3.20) gives

$$-\kappa^{3/2}\left(\kappa\,\frac{\theta_i+\Gamma_e\sqrt{8}}{\theta_u+\Gamma_e\sqrt{8}}\right)^{1/4}=\left[\left(\frac{s_0-\sigma_i}{s_0-\sigma_i+h}\right)^{1/4}\left(1+\frac{\pi\sqrt{8}}{3}\frac{1}{\kappa}\right)-\frac{\pi\sqrt{8}}{3}\frac{1}{\kappa}\left(\frac{s_2-\sigma_u+h}{s_2-\sigma_u}\right)^{1/4}\right] \tag{4.3.26}$$

$$-\kappa^{3/2}\left(\kappa\,\frac{\theta_i+e^{\sqrt{8}}}{\theta_u+\Gamma_e\sqrt{8}}\right)^{-1/4}=\left[\left(\frac{s_2-\sigma_i}{s_2-\sigma_u+h}\right)^{1/4}\left(1+\frac{\pi\sqrt{8}}{3}\frac{1}{\kappa}\right)-\frac{\pi\sqrt{8}}{3}\frac{1}{\kappa}\left(\frac{s_2-\sigma_u+h}{s_2-\sigma_u}\right)^{1/4}\right] \tag{4.3.27}$$

Let $X=\left(\frac{s_0-\sigma_i}{s_0-\sigma_i+h}\right)^{1/4}$, $\quad 0<X<1$

$Y=\left(\frac{s_2-\sigma_u}{s_2-\sigma_u+h}\right)^{1/4}$, $\quad 0<Y<1$

(4.3.26) and (4.3.27) become

$$-K=X\left(1+\frac{\pi\sqrt{8}}{3}\kappa\right)-\frac{\pi\sqrt{8}}{3}KX^{-1} \tag{4.3.28}$$

$$-\frac{1}{K}=Y\left(1+\frac{\pi\sqrt{8}}{3}\frac{1}{\kappa}\right)-\frac{\pi\sqrt{8}}{3}\frac{1}{K}Y^{-1} \tag{4.3.29}$$

where $$K=\kappa^{3/2}\left(\kappa\,\frac{\theta_i+\Gamma_e\sqrt{8}}{\theta_u+\Gamma_e\sqrt{8}}\right)^{1/4}$$

Since $\kappa=\frac{\theta_i}{-\theta_u}$ we have, with $\frac{\Gamma_u}{\Gamma_i}=\mu$,

$$K=\kappa^{7/4}\left\{\frac{(\kappa+\sqrt{8})+\kappa(\sqrt{8}-1)\mu}{(\sqrt{8}-1)+(\kappa\sqrt{8}+1)\mu}\right\}^{1/4}$$

(4.3.28) and (4.3.29) give

$$X=\frac{-K+\sqrt{K^2+\frac{4}{3}\pi\sqrt{8}\,K\left(1+\frac{1}{3}\pi\sqrt{8}\,K\right)}}{2\left(1+\frac{1}{3}\pi\sqrt{8}\,K\right)} \tag{4.3.30}$$

$$Y=\frac{-1/\kappa+\sqrt{1/K^2+\frac{4}{3}\pi\sqrt{8}\,\frac{1}{K}\left(1+\frac{1}{3}\pi\sqrt{8}\,K\right)}}{2\left(1+\frac{1}{3}\pi\sqrt{8}\,\frac{1}{K}\right)} \tag{4.3.31}$$

From (4.3.25) follows

$$\left(\frac{R_i}{R_u}\right)^2 = \frac{1}{\kappa^3}\,\frac{s_2 - \sigma_u}{s_0 - \sigma_i} = \frac{1}{\kappa^3}\,\frac{Y^4}{X^4}\,\frac{1-X^4}{1-Y^4} \qquad (4.3.32)$$

Equations (4.3.30) - (4.3.32) contain only the unknown Γ_e (via κ). For every value of Γ_e ($\Gamma_i > \Gamma_e > \Gamma_u$) for given μ equations (4.3.30)-(4.3.32) give a value for $\frac{R_i}{R_u}$.

4.4 Comparison with experiment

A comparison will be made with the very precise measurements taken by Donnelly (1958). In Donnelly's experiments the outer cylinder is at rest, i.e. $\mu = 0$. Measurements were taken with $R_i/R_u = 1.9/2.0 = 0.95$ and $R_i/R_u = 1/2$. With $\mu = 0$ equations (4.3.30) - (4.3.32) give $R_i/R_u = 0.50$ for $\kappa = 1.83$, $R_i/R_u = 0.95$ for $\kappa = 1.155$. Consider first the case $R_i/R_u = 0.50$, $\kappa = 1.83$. One obtains $X^4 = 0.2625$, $Y^4 = 0.3335$ (using (4.3.30) and (4.3.31). Hence

$$s_0 - \sigma_i = \frac{X^4}{1-X^4} = 0.356\,h$$

$$s_2 - \sigma_u = \frac{Y^4}{1-Y^4}\,h = 0.500\,h$$

Substitution in (4.3.21) and (4.3.22) gives

$$M_1 = 1.972\,\Gamma_i^{3/2}\,h^{1/2}\,T^{-1/4}$$

$$M_3 = -0.296\,\Gamma_i^{3/2}\,h^{1/2}\,T^{-1/4}$$

The dimensionless torque G due to one vortex cell equals $M_1 - M_3$, hence

$$G = 2.268\ T^{-1/4}\ \Gamma_i^{3/2}\ h^{1/2}$$

With the outer cylinder at rest the reference velocity in the present case ($\Gamma_u^* = 0$, $d^* = R_i^*$) is Γ_i^*/R_i^*, the reference length is $d^* = R_i^*$. Hence the dimensional torque is

$$G^* = 2.268\ n\rho\Gamma_i^{*2} R_i^* \left(\frac{h^*}{d^*}\right)^{1/2} \frac{\nu_i^{1/2}}{\Omega_i^{*2} R_i^*} = 2.268\ n\rho\nu^{1/2} \left(\frac{h^*}{R_i^*}\right)^{1/2} R_i^{*4} \Omega_i^{*3/2} \qquad (4.4.1)$$

where n is the total number of cells. This number is unknown. The simplest assumption would be that the number of cells does not change as the Taylor number is increased, and is therefore equal to the number of cells near T_c. This number can be found from the wave-number of the cells (i.e. $a = \pi R_u/h$) at $T = T_c$ which is given by hydrodynamic stability theory, (e.g. Chandrasekhar, 1961, pp. 323, 304).

The cell-structure has been explored experimentally in great detail for a wide range of supercritical Taylor numbers by Donald Coles (1965). This investigation shows (see Coles' Fig. 13) that if the gap between the Cylinders is small the wave-number tends to decrease as T increases, i.e. the height h of the cells increases. It should be noted that if the gap between the cylinders is small the flow varies periodically in the azimuthal direction also for $T > 1.2\ T_c$ (outer cylinder at rest). The cells take on a "wavy" shape. But for wider gaps ($R_u/R_i = 2$ for instance) the flow remains rotationally symmetric even for values of T much larger than T_c. Therefore it remains to be seen whether also in the case of a wide gap the cell height tends to increase as T increases.

For the time being it is assumed here that the dimensions of

the cells do not change as T increases. Chandrasekhar gives for the wave-number at $T = T_c$ $(R_u/R_i = 2)$ $a = 6.2$, therefore $h = 0.49\, R_u$. For Donnelly's wide gap experiment this would give $h^* = 0.98$ cm. It seems there can only be an even number of cells. Since the total length of Donnelly's cylinders was 10 cm. one obtains 10 as the most likely number of cells, with $h^* = 1$ cm. Because the suspended part of the cylinder on which Donnelly measured torque was 5 cm. long 5 cells contribute to the torque. Hence one obtains for the torque

$$G^* = 11.34\, \rho \nu^{1/2} R_i^{*4} \Omega_i^{*3/2}$$

or

$$\frac{2\pi \cdot 10^3}{\rho \Omega_i^{*2}} G^* = 28{,}400 \left(\frac{\Omega_i^*}{2\pi\nu}\right)^{-1/2} \qquad (4.4.2)$$

This relation has been plotted in Fig. 4. The rest of Fig. 4 has been taken from Donnelly's paper. At $\Omega_i^*/2\pi\nu = 100$ $(T = 100\, T_c)$ the measurements give

$$\frac{2\pi \cdot 10^3}{\rho \Omega_i^{*2}} G^* = 2200$$

whereas (4.4.1) gives

$$\frac{2\pi \cdot 10^3}{\rho \Omega_i^{*2}} G^* = 2840$$

which is 29% higher. If the cell height is taken larger this difference decreases.

In the same way one obtains for the case $R_i/R_u = 0.95$

$$G^* = 0.747\, n \rho \nu^{1/2} \left(\frac{h^*}{R_i^*}\right)^{1/2} R_i^{*4}\, \Omega^{*3/2}$$

Chandrasekhar gives $\pi\frac{d}{h} = 3.12$, hence $h^* \cong R_u^* - R_i^*$. For Donelly's narrow gap experiment this gives $h^* = 0.1$ cm., 50 cells contribute to the torque. The result is

$$\frac{2\pi \cdot 10^3}{\rho\Omega_i^{*2}} G^* = 28.1 \cdot 10^4 \left(\frac{\Omega_i^*}{2\pi\nu}\right)^{-1/2} \qquad (4.4.3)$$

For the narrow gap case Coles gives an "expected state" according to which at high Taylor numbers the cell height is 1.25 times that at the critical Taylor number. This gives

$$\frac{2\pi \cdot 10^3}{\rho\Omega_i^{*2}} G^* = 25.2 \cdot 10^4 \left(\frac{\Omega_i^*}{2\pi\nu}\right)^{-1/2} \qquad (4.4.4)$$

Relations (4.4.3) and (4.4.4) have been represented graphically in Fig. 5 (curves A and B respectively). At $\Omega_i^*/2\pi\nu = 10^3$ the measurements give

$$\frac{2\pi \cdot 10^3}{\rho\Omega_i^{*2}} G^* = 0.70 \cdot 10^4$$

whereas (4.4.2) gives

$$\frac{2\pi \cdot 10^3}{\rho\Omega_i^{*2}} G^* = 0.89 \cdot 10^4 \quad (27\% \text{ higher})$$

and (4.4.3) gives

$$\frac{2\pi \cdot 10^3}{\rho\Omega_i^{*2}} G^* = 0.79 \cdot 10^4 \quad (14\% \text{ higher})$$

It should be kept in mind that in this case the actual flow has azimuthal oscillations. These have not been taken into account in the present approximate calculations.

It is clear from Fig. 4 that the slopes of the experimental and theoretical curves are unequal as $\Omega_i^* \to \infty$. The cause of this discrepancy does not lie in the approximations made in the preceding calculations. The proportionality

$$\frac{G^*}{\rho\Omega_i^{*2}} \propto \left(\frac{\Omega_i^*}{2\pi\nu}\right)^{-1/2}$$

can be derived by straightforward dimensional analysis, as shown by

Batchelor in an appendix to a paper by Donnelly and Simon (Batchelor, 1960). The fact that the slope of the experimental curve differs a little from this theoretical prediction is somewhat disturbing.

Batchelor's complete result based on dimensional analysis is, with minor changes in notation,

$$G \propto \rho H^* R_i^{*4} \Omega_i^{*2} \left(\frac{\Omega_i^* R_i^* d^*}{\nu}\right)^{1/2} \left(\frac{d^*}{R_i^*}\right)^{1/4} \tag{4.4.5}$$

where H^* is the total length of the cylinders. In the preceding theory the dependence of G^* on d^* is implicit in the complicated algebraic relations which connect κ with R_i/R_u; this dependence cannot be expressed in simple form. Donnelly and Simon (1960) made an excellent survey of torque measurements. They fitted a curve given by

$$\frac{G^*}{\rho H^* \Omega_i^{*2} R_i^{*4}} \propto \left(\frac{\Omega_i^* R_i^* d^*}{\nu}\right)^{-\ell} \left(\frac{d^*}{R_i}\right)^m \tag{4.4.6}$$

with experimental results and find $\ell \doteqdot 0.62$, $m = 0.32 \pm 0.05$. These results are consistent with (4.4.5), but the spread in m seems to indicate that in reality the dependence of G^* on d^* is more complicated than (4.4.5).

Batchelor assumed that the height h^* of the cells equals h^* at $T=T_c$. This makes h^* a function of d^* (keeping the outer cylinder at rest). Therefore (4.4.5) does not give a dependence of G^* on h^*.

The agreement between the foregoing approximate torque calculations and experiment is close enough to lend strong support to the preceding theoretical description of the flow.

A final remark concerns Snyder's and Lambert's observation that the outward flow resembles a thin jet (as has been deduced in this

thesis) but the inward flow is slow (contrary to the present theoretical description). Taking the case $R_u/R_i = 2$ we have $\kappa = 1.83$. With the outer cylinder at reat it follows from the definition of κ that $\theta = \frac{\kappa}{\kappa+1}\Gamma_i = 0.646$ (from the choice of reference quantities follows $\Gamma_i = 1$)

$$\Gamma_e = -\theta_u = +\frac{\Gamma_i}{\kappa+1} = 0.353$$

Substitution in (4.1.13) gives for the magnitude of the dimensionless velocity at the points of impingement:

$$S_2 = 0.863$$

$$S_4 = 0.414$$

Hence the inward moving shear layer is remarkably slower than the outward moving layer, which may account for the observation of a slow inflow by Snyder and Lambert.

5. Conclusion

It has been shown that a boundary layer type flow model whereby the Taylor-vortex cell consists of an inviscid core surrounded by a thin viscous region results in a self-consistent description of the flow. The model leads directly to a simple explanation of the mechanism by which strongly developed Taylor vortices are driven. Approximate calculations of the torque agree well enough with experiment to lend strong support to this flow model. For more accurate calculations of the torque at high Taylor numbers equations (2.8) and (2.10) must be solved numerically.

Appendix 1.

A discussion of the state problem.

In the foregoing calculations the height of the cells is arbitrary and must be given before the flow field can be calculated. In the following a short review is given of publications concerning the determination of the height of the cells.

By "the state problem" we mean the determination of the state of the flow, that is, the determination of the height of the cells. If there are azimuthal variations ("wavy" vortices) the determination of the state of the flow includes a specification of the wavelength of the azimuthal waves. Azimuthal waves occur at Taylor numbers only slightly above the critical Taylor number if the gap between the cylinders is small ($d/R_i = 1/10$ say) (Coles, 1965). For $d/R_i = 1$ experiment indicates that azimuthal waves do not occur at all (Snyder and Lambert (1966)).

The state problem has not yet been solved theoretically. The present work would have contributed to the solution of the state problem if the boundary layer equations (2.10) had been solved more accurately (analytically or numerically). Presumably, for cell heights either too great or too small a physically admissible solution of (2.10) might not exist. For cell heights too large it seems fairly certain that the boundary layers on the cylinder walls will separate before reaching the corners of the cell. For cell heights too small (2.10) may not have a single-valued solution. Or perhaps, single-valued solutions exist only for discrete values of the cell height. In any event, the state problem cannot be solved completely by studying the asymptotic behavior of the solutions

as $T \to \infty$ more accurately, if the solutions are not unique. At most, one can determine which states are possible.

In the case of a small gap experiment strongly indicates non-uniqueness (Coles, 1965), i.e. for a given Taylor number more than one state can be realized experimentally. For $R_u/R_i = 2$ experiment indicates that the cell height tends to increase with T (Donnelly and Schwarz, 1965; Snyder and Lambert, 1966). On the uniqueness question these experiments do not throw much light. Numerical calculations (Meyer, 1966) indicate non-uniqueness.

Much theoretical work has been done on the state problem. A state problem also occurs in the flow in a horizontal layer of fluid heated from below (Bénard flow). If the Rayleigh number Ra exceeds a critical value buoyance forces set up a flow pattern which may consist of two-dimensional rolls or hectagonal cells (Bénard cells). If the layer of fluid is bounded above and below not by rigid walls but by fluid the flow which occurs for $Ra = Ra_{crit}$ takes a form which is analytically very simple: it is described by trigonometric and hyperbolic functions. For this reason investigations of the non-linear régime ($Ra > Ra_{crit}$) are simpler for this flow than for Taylor-vortex flow. Hence greater progress has been made. Of course there is no direct relationship between the state problem for Bénard flow and for Taylor-vortex flow, but theoretical ideas and methods designed to penetrate into the non-linear régime of Bénard flow may be expected to apply to Taylor-vortex flow as well, and vice-versa. For this reason a short survey of work on the state problem for Bénard flow will be given.

Malkus and Veronis (1958) showed that the equations have

many solutions for $Ra > Ra_{crit}$, but that only those solutions are stable against disturbances which have the form of the other solutions which maximize the heat transport. The question of how many solutions maximize the heat transport is left unanswered.

Another investigation connected with the state problem for Bénard flow is the work by Segel (1962). This paper considers the interaction of two "roll" disturbances with different wavelengths for $Ra > Ra_{crit}$, assuming that the fluid is initially at rest. Because of this assumption Segel's work has no direct connection with physical reality (the fluid cannot be at rest for $Ra > Ra_{crit}$) but it provides valuable insight in the mathematical properties of the non-linear equations which describe the problem. Such an interaction of two disturbances was first studied by Palm (1960) whose work was later modified and refined by Segel and Stuart (1962). According to Segel's analysis, two infinitesimal disturbances, both of which would be amplified according to linearized theory, interact in such a way that only one of them remains. Which one depends on the relative magnitude of their initial amplitudes, which are prescribed. This result is reminiscent of Coles' experiment, in which the state which is realized depends on the way the experimenter has varied the speed of the cylinders before a steady state is obtained.

Turning now to the Taylor-vortex flow problem, an important mathematical result has been derived by W. Velte (1965). It is shown that at $T = T_c$ there is a branching of stationary solutions of the Navier-Stokes equations. The question whether the new branch exists for $T < T_c$ or for $T > T_c$, and how many branches come together at $T = T_c$, is left unanswered. This is the only published theoretical

paper on the state problem for Taylor-vortex flow.

Note. The state problem is also studied in an unpublished paper by Reynolds and Potter (1967), which was brought to the author's attention by Prof. Coles. Assuming axial symmetry, finite amplitude solutions are developed as powers of $(T^{1/2} - T_c^{1/2})$. This has also been done by Davey (1962). It turns out that there is an infinite number of solutions. Reynolds and Potter study the stability of these solutions, and it is found that only one solution is stable. This solution has the property that its wave-length (cell height) decreases with T.

Contrary to the claims of the authors, however, they have not solved the state problem in this way, because their results depend on an important assumption, which is not stated and which remains to be justified. Reynolds and Potter perturb their finite amplitude solutions with a perturbation which depends on time like e^{gt}. They argue that for a stable finite amplitude solution (with wavelength $\lambda = \lambda_s$) $g = 0$, thereby assuming that solutions with λ slightly less and slightly higher than λ_s will be unstable $(g > 0)$, so that the case $g < 0$ does not occur. In other words, Reynolds and Potter assume a priori that the spectrum of possible states is discrete. Stable solutions are assumed to exist only for discrete values of λ_s; solutions with λ inbetween these values are unstable. Only one possible value of λ_s is found.

It is clear that the assumption of a discontinuous spectrum needs to be justified. If it turns out that in reality the spectrum is

continuous then Reynolds and Potter have not determined the only possible finite amplitude solution, but the marginal stability boundary (I) of the spectrum of finite amplitude solutions (see Fig. 6). In that case there should be a second marginal stability boundary (II), which however was not found by Reynolds and Potter. Before this is taken as proof that the spectrum is indeed discrete a detailed investigation of the possibility of branching of the marginal stability boundary seems called for. The branching of the marginal stability boundary may have been masked by the asymptotic method used by Reynolds and Potter.

The most striking result of Reynolds' and Potter's theory is the absence of non-uniqueness. If this result is correct the non-uniqueness observed experimentally in the case of a small gap (Coles, 1965) must be due to the azimuthal waves. In the case $R_u/R_i = 2$, where azimuthal waves are absent experiment should show no non-uniqueness at all. It has already been mentioned that at present there are no experimental results available which settle this question conclusively. Meyer's (1966) numerical calculations show non-uniqueness.

Reynolds' and Potter's prediction of decreasing wave-length with increasing T is somewhat at variance with experiment. Donnelly and Schwarz (1965) and Snyder and Lambert (1966) find a (not very pronounced) trend of increasing wavelength with increasing T, with $R_u/R_i = 2$.

Appendix 2.

Derivation of the meridional and angular momentum-integral equations.

Equations (4.1.2) and (4.1.3) can easily be derived as follows: (2.10a) can be written as

$$rU\frac{\partial}{\partial s}(U-U_e)+rW\frac{\partial}{\partial n}(U-U_e)+r(U-U_e)\frac{dU_e}{ds}=\frac{\Gamma^2-\Gamma_e^2}{r^2}\frac{dr}{ds}+T^{-\frac{1}{2}}r\frac{\partial^2 U}{\partial n^2} \qquad (A.1)$$

Multiplying (2.10c) with $(U-U_e)$ and adding to (A.1) gives:

$$\frac{\partial}{\partial s}\left\{rU(U-U_e)\right\}+\frac{\partial}{\partial n}\left\{rW(U-U_e)\right\}+r(U-U_e)\frac{dU_e}{ds}=\frac{\Gamma^2-\Gamma_e^2}{r^2}\frac{dr}{ds}+T^{-\frac{1}{2}}r\frac{\partial^2 U}{\partial n^2} \qquad (A.2)$$

Integration of this equation with respect to n between $n=0$ and $n=\infty$, taking into account that $W=\frac{\partial U}{\partial n}=0$ at $n=0$, $U-U_e=\frac{\partial U}{\partial n}=0$ at $n=\infty$ gives equation (4.1.2).

Equation (2.10b) can be written as

$$rU\frac{\partial}{\partial s}(\Gamma-\Gamma_e)+rW\frac{\partial}{\partial n}(\Gamma-\Gamma_e)=T^{-\frac{1}{2}}r\frac{\partial^2\Gamma}{\partial n^2} \qquad (A.3)$$

Multiplying (2.10c) with $(\Gamma-\Gamma_e)$ and adding to (A.3) gives

$$\frac{\partial}{\partial s}\left\{rU(\Gamma-\Gamma_e)\right\}+\frac{\partial}{\partial n}\left\{rW(\Gamma-\Gamma_e)\right\}=T^{-\frac{1}{2}}r\frac{\partial^2\Gamma}{\partial n^2} \qquad (A.4)$$

Integration of this equation with respect to $n=0$ and $n=\infty$, taking into account that $W=\frac{\partial\Gamma}{\partial n}=0$ at $n=0$, $\Gamma-\Gamma_e=\frac{\partial\Gamma}{\partial n}=0$ at $n=\infty$ gives equation (4.1.3).

Appendix 3.

The solution for the inviscid core.

The flow in the inviscid core is governed by equation (2.8):

$$\left.\begin{aligned} r\frac{\partial}{\partial r}\left(\frac{1}{r}\frac{\partial\psi}{\partial r}\right)+\frac{\partial^2\psi}{\partial z^2} &= Cr^2 \\ rv &= \Gamma_e \end{aligned}\right\} \qquad (A.5)$$

The boundary conditions are, taking $z = 0$ in the middle of a cell:

$$\psi = 0 \quad \text{for} \quad r = R_i,\ r = R_u,\ z = \pm\frac{h}{2} \qquad (A.6)$$

Let
$$\psi = \overline{\psi} + \frac{C}{8}\left(r^2-R_i^2\right)\left(r^2-R_u^2\right), \qquad (A.7)$$

then
$$\frac{\partial^2\overline{\psi}}{\partial r^2} - \frac{1}{r}\frac{\partial\overline{\psi}}{\partial r} + \frac{\partial^2\overline{\psi}}{\partial z^2} = 0 \qquad (A.8)$$

The following boundary conditions are satisfied by $\overline{\psi}$:

$$\overline{\psi} = 0 \quad \text{for} \quad r = R_i\ ,\ r = R_u \qquad (A.9a)$$

$$\overline{\psi} = \frac{C}{8}\left(r^2-R_i^2\right)\left(R_u^2-r^2\right) = F(r) \quad \text{for} \quad z = \pm\frac{h}{2} \qquad (A.9b)$$

Separation of variables gives

$$\left.\begin{aligned} \overline{\psi} &= R(r)\,Z(z) \\ R'' - \frac{1}{r}R' - cR &= 0 \\ Z'' + cZ &= 0 \end{aligned}\right\} \qquad (A.10)$$

In order to satisfy boundary condition (A.9a) we must have $R(R_i) = R(R_u) = 0$. It turns out that this is only possible if the constant c is negative. Writing $c = -\gamma_n^2$,

$$\left.\begin{aligned} R'' - \frac{1}{r}R' + \gamma_n^2 R = 0 \\ R(R_i) = R(R_u) = 0 \end{aligned}\right\} \qquad (A.12)$$

Equation (A.12) is of the Sturm-Liouville type and there are infinitely many eigenvalues γ_n and infinitely many eigenfunctions $R = R_n$. Moreover, these eigenfunctions form a complete set so that the function $F(r)$ in boundary condition (A.9b) can be represented as a linear combination of the R_n's. The solution for R_n is found to be

$$R_n = r\left\{J_1(\gamma_n r)\, Y_1(\gamma_n R_i) - J_1(\gamma_n R_i)\, Y_1(\gamma_n r)\right\}$$

with γ_n defined by (A.13)

$$J_1(\gamma_n R_u)\, Y_1(\gamma_n R_i) - J_1(\gamma_n R_i) Y_1(\gamma_n R_u) = 0$$

The relevant solution of (A.11) is

$$Z = Z_n = \cosh(\gamma_n z) \qquad (A.14)$$

The solution for $\overline{\psi}$ is built up by superposition of the functions $R_n Z_n$:

$$\overline{\psi} = \sum_1^\infty A_n \cosh\left(\gamma_n z\right) r\left\{J_1(\gamma_n r)\, Y_1(\gamma_n R_i) - J_1(\gamma_n R_i) Y_1(\gamma_n r)\right\} \qquad (A.15)$$

The constant γ_n has been chosen such that the boundary condition (A.9a) is satisfied. The boundary condition (A.9b) is satisfied if

$$F(r) = \sum_1^\infty A_n \cosh\left(\gamma_n \frac{h}{2}\right) r\, C_{1,1}(\gamma_n r) \qquad (A.16)$$

where

$$C_{1,1}(\gamma_n r) = J_1(\gamma_n r)\, Y_1(\gamma_n R_i) - J_1(\gamma_n R_i) Y_1(\gamma_n r)$$

According to the discussion following equation (A.12) it is indeed possible to represent $F(r)$ in this way. The constants are given by

$$A_n = \frac{1}{R_u^2 N_n \cosh\left(\gamma_n \frac{h}{2}\right)} \int_{R_i}^{R_u} F(r)\, C_{1,1}(\gamma_n r)\, dr \qquad (A.17)$$

where $$N_n = \frac{2}{\pi^2 \gamma_n^2 R_u^2} \left[\frac{J_1^2(\gamma_n R_i)}{J_1^2(\gamma_n R_u)} - 1 \right]$$

A proof of this result has been given by Titchmarsh (1923). By partial integration one finds

$$A_n = \frac{\pi C R_u^3}{\gamma_n^2 R_u^2 \cosh\left(\gamma_n \frac{h}{2}\right)} \frac{J_1(\gamma_n R_u)\left\{\frac{R_i}{R_u} J_1(\gamma_n R_u) - J_1(\gamma_n R_i)\right\}}{J_1^2(\gamma_n R_u) - J_1^2(\gamma_n R_i)} \qquad (A.18)$$

The values of γ_1, γ_2 and γ_3 have been tabulated by Chandrasekhar and Elbert (1954). For the case $R_u/R_i = 2$ the following result is obtained:

$$\begin{pmatrix} A_1 \\ A_2 \\ A_3 \end{pmatrix} = \frac{C R_u^3}{8 \cosh\left(\gamma_n \frac{h}{2}\right)} \begin{pmatrix} -1.134 \\ 0.143 \\ -0.134 \end{pmatrix} \qquad (A.19)$$

Using equations (A.7), (A.15) and (A.19) one finds that the extremum of ψ and hence the center of the vortex flow pattern is closer to the outer cylinder than to the inner cylinder. This fact has been taken into account in the qualitative flow picture in Fig. 1.

In order to obtain some more information about the flow pattern the radial velocity u at the edge of a cell has been computed

with $R_i = 1$, $R_u = 2$, $h = 1$ (cell cross-section square). At the edge of a cell $z = \frac{1}{2}$ in the present case, and one obtains

$$u(r, \tfrac{1}{2}) = \left(\frac{1}{r}\frac{\partial \psi}{\partial z}\right)_{z=1/2} = \sum_{1}^{\infty} A_n \gamma_n \sin h \frac{\gamma_n}{2} \left\{ J_1(\gamma_n r) Y_1(\gamma_n) - J_1(\gamma_n) Y_1(\gamma_n r) \right\} \quad \text{(A.20)}$$

It is clear that the corners $(r = 1, r = 2)$ are stagnation points. The sum of the first three terms of this series has been plotted in Fig. 7.

References

Batchelor, G. K., 1956, J. Fluid Mech. 1, 177.

Batchelor, G. K., 1960, J. Fluid Mech. 7, 416

Chandrasekhar, S., 1961, Hydrodynamic and hydromagnetic stability, Oxford 1961.

Chandrasekhar, S., and Elbert, D., 1954, Proc. Camb. Phil. Soc. 50 266.

Coles, Donald, 1965, J. Fluid Mech. 21, 385.

Coles, Donald, 1967, A note on Taylor instability in circular Couette flow (to be published in J. App. Mech.)

Couette, M., 1890, Ann. Chim. Phys. (6) 21, 433.

Davey, A., 1962, F. Fluid Mech. 14, 336.

Donnelly, R. J., 1958, Proc. Roy. Soc. A, 246, 312.

Donnelly, R. J., and Simon, N. J., 1960, J. Fluid Mech., 7, 401.

Donnelly, R. J., and Schwarz, K. W., 1965, Proc. Roy. Soc. London, A. 283, 531.

Feynman, R. P. and Lagerstrom, P. A., 1956, Remarks on high Reynolds number flows in finite domains, IX Intern, Congr. App. Mech., Brussels, 1956.

Glauert, M. B., 1956, J. Fluid Mech., 1, 625.

Goldstein, S., Lectures on Fluid Mechanics, Interscience, 1960.

Lagerstrom, P. A. and Cole, J. D., 1955, J. Rat. Mech. Anal. 4, 817.

Malkus, W. V. R., and Veronis, G., 1958, J. Fluid Mech. 4, 225.

Meyer, K. A., 1966, A two-dimensional time-dependent numerical study of rotational Couette flow. Los Alamos Rep. LA 3497

Palm, E., 1960, J. Fluid Mech., 8, 183.

Prandtl, L., 1961, Gesammelte Abhandlungen, Springer, 1961.

Lord Rayleigh, 1916, On the dynamics of revolving fluids, Scientific papers, 449, Dover, 1964.

References, cont'd.

Reynolds, W. C. and Potter, M. C., 1967, A finite amplitude state-selection theory for Taylor-vortex flow. (unpublished).

Segel, L. A. and Stuart, J. T., 1962, J. Fluid Mech. 13, 289.

Segel, L. A., 1962, J. Fluid Mech., 14, 97.

Snyder, H. A. and Lambert, R. B., 1966, J. Fluid Mech., 26, 545.

Stuart, J. T., 1958, J. Fluid Mech., 4, 1-21.

Taylor, G. I., 1923, Phil. Trans. A. 223, 289-343.

Titchmarsh, E. C., 1923, Proc. London Math. Soc. 22, xiii.

Velte, W., 1965, Report DLR Fb 65-61.

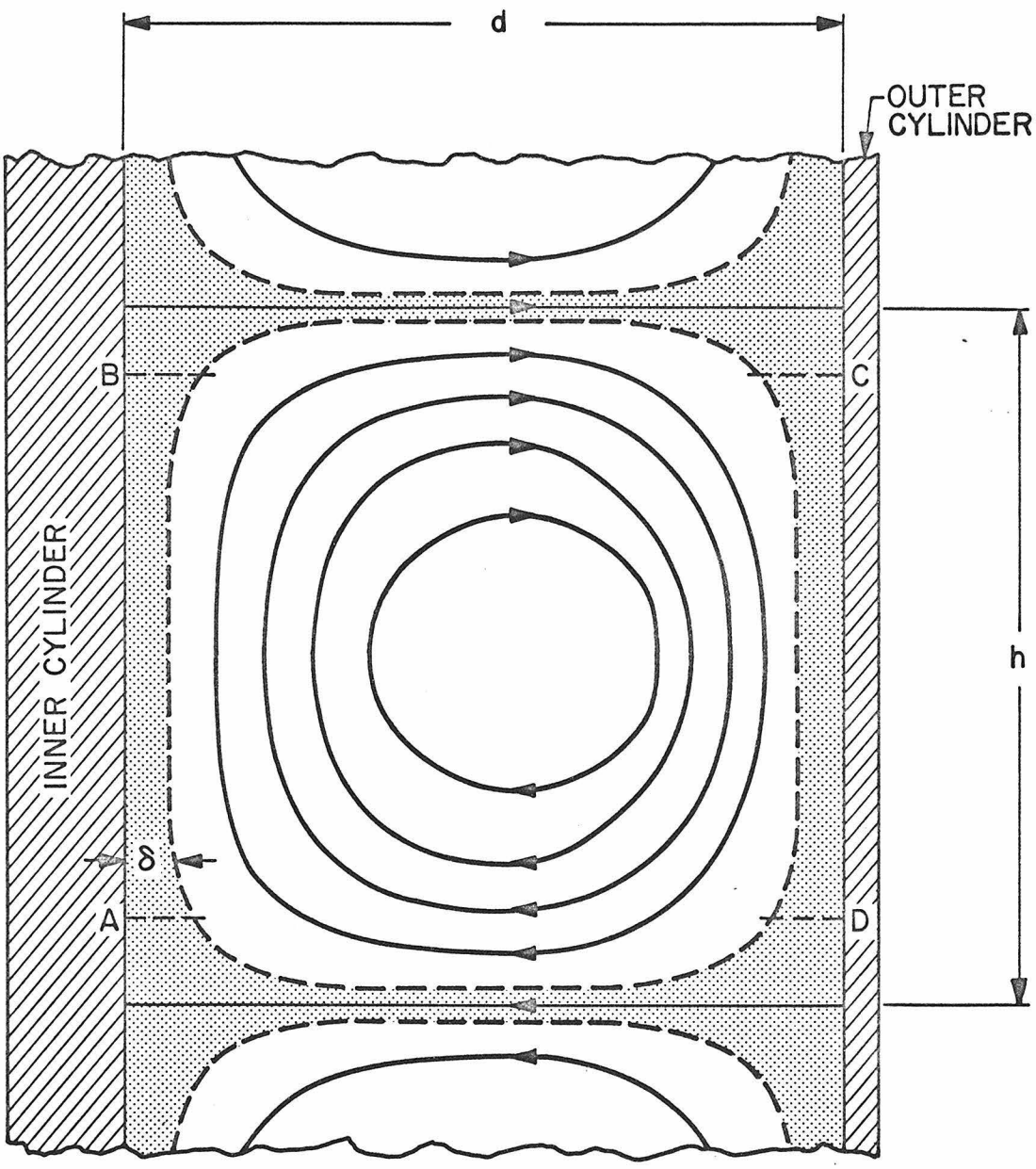

Figure 1. Sketch of the flow in an axial plane. The shaded area represents the region in which viscous forces are important.

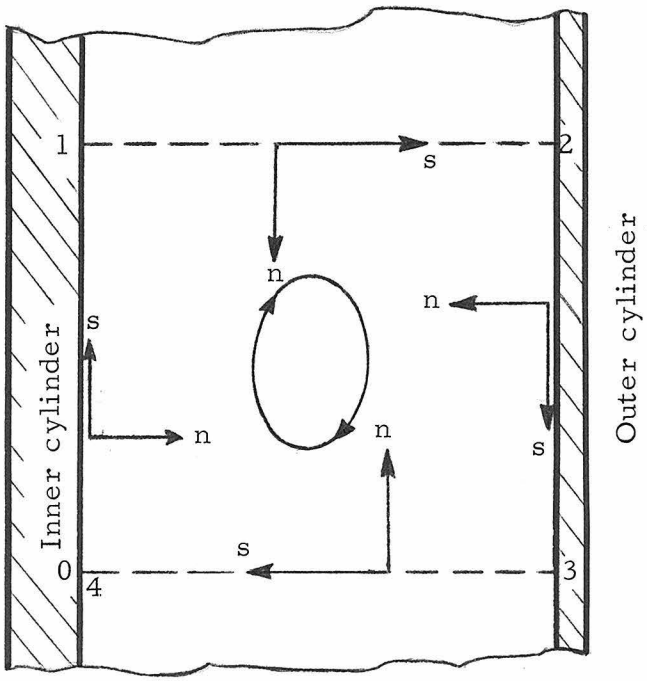

Figure 2. Definition of the coordinate system (s,n) for the viscous region.

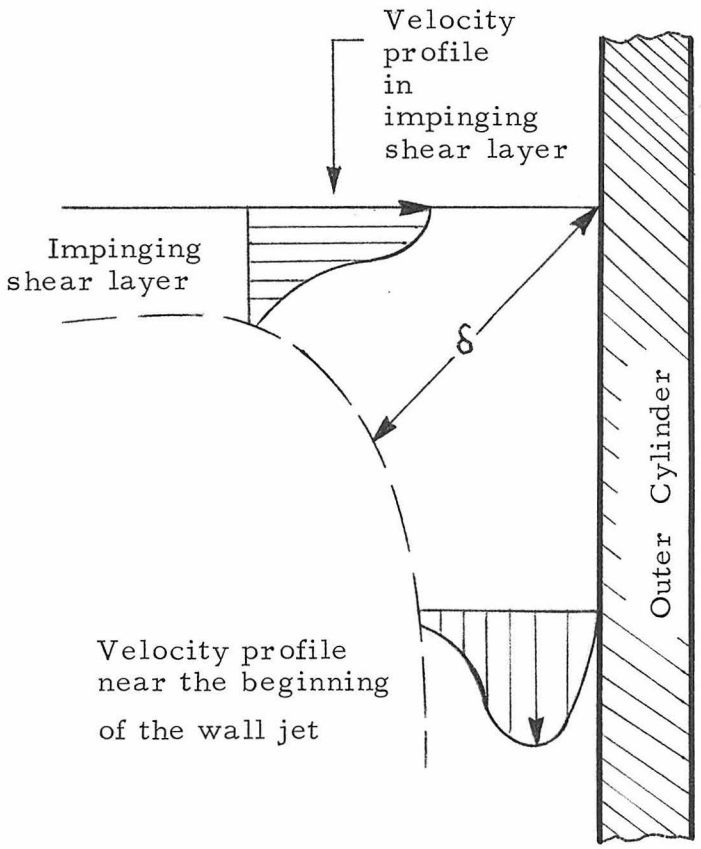

Figure 3. Sketch of velocity profiles near a point of impingement.

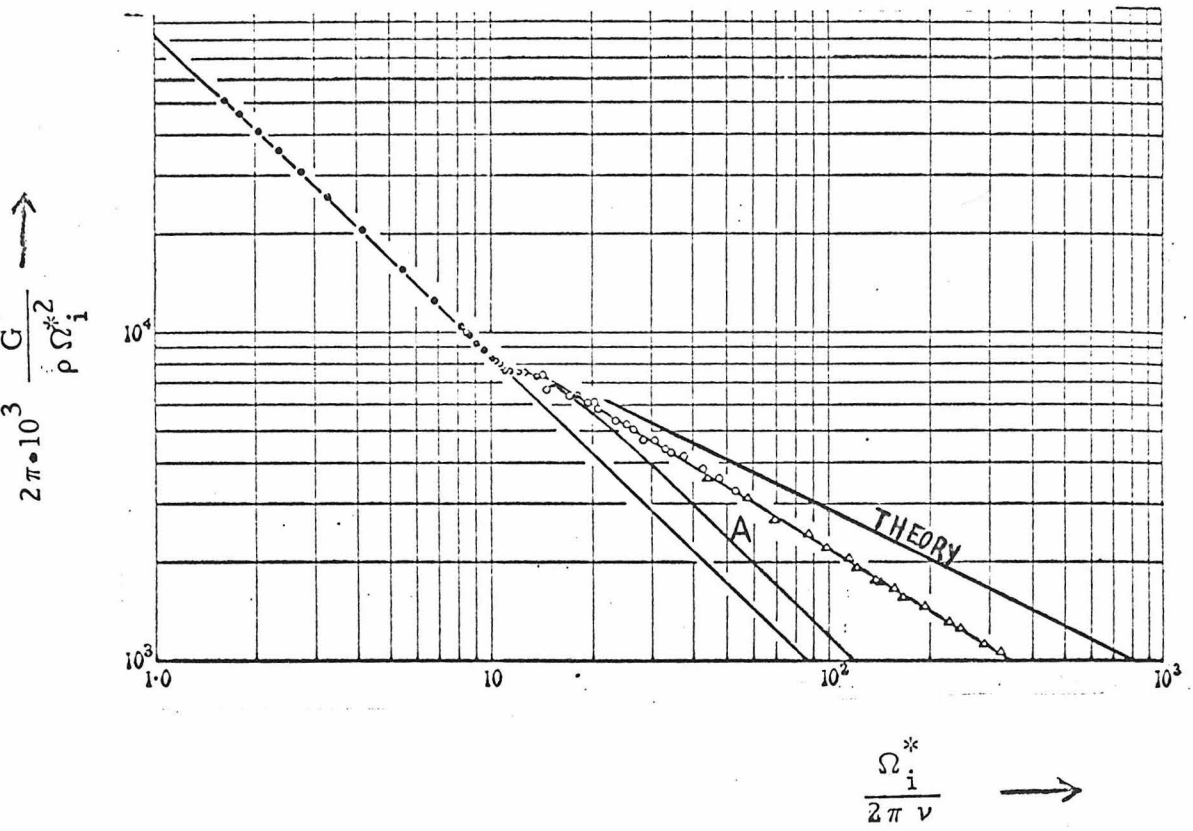

Figure 4. Comparison with experiment. The circles and triangles represent measurements taken by Donnelly (1958, fig. 8) with R_i = 1.0 cm., R_u = 2.0 cm. The theoretical curve is given by equation (4.4.2). Curve A represents Davey's (1962) theory.

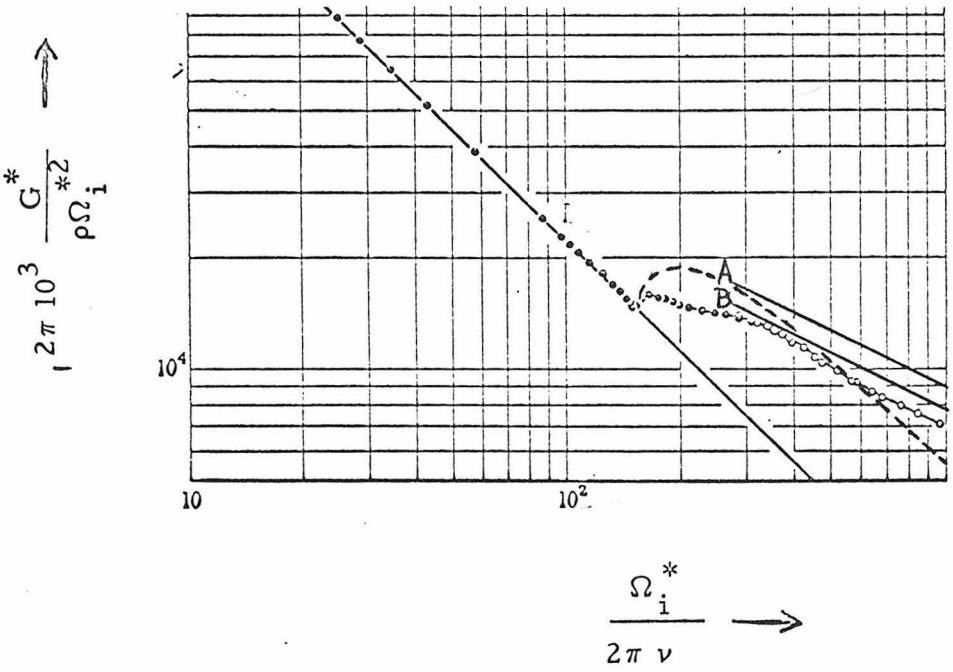

Figure 5. Comparison with experiment. The circles represent measurements taken by Donnelly (1958, fig. 5) with $R_i = 1.9$ cm., $R_u = 2.0$ cm. The theoretical curves A and B are given by equations (4. 4. 3) and (4. 4. 4) respectively. The dashed curve represents Davey's (1962) theory.

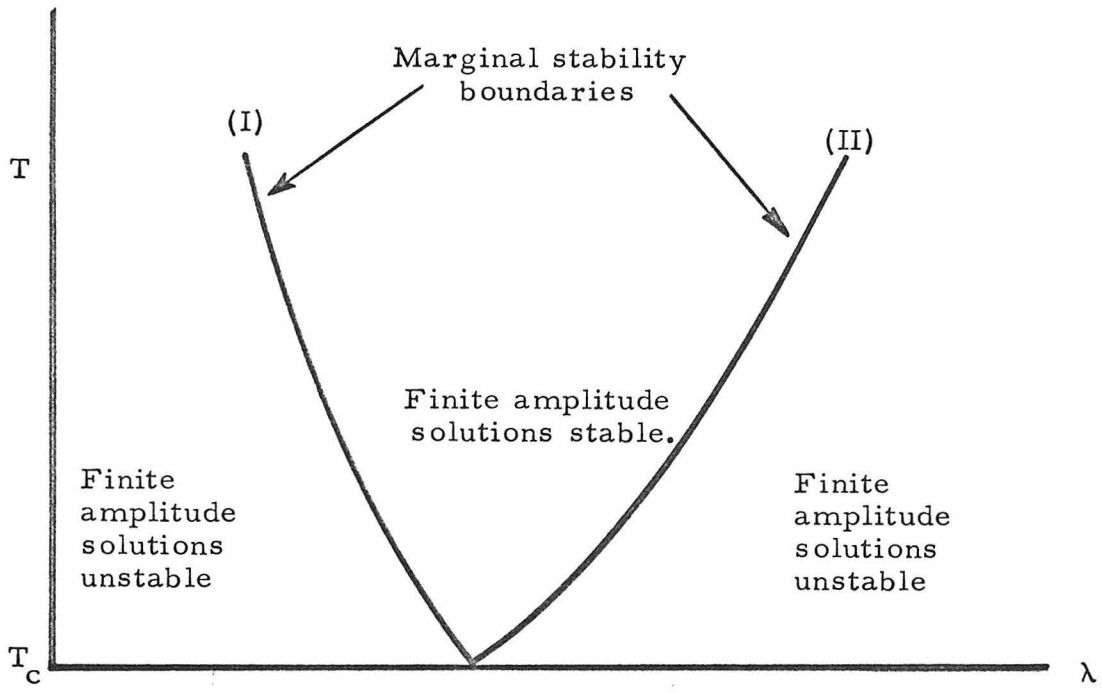

Figure 6. The marginal stability boundaries.

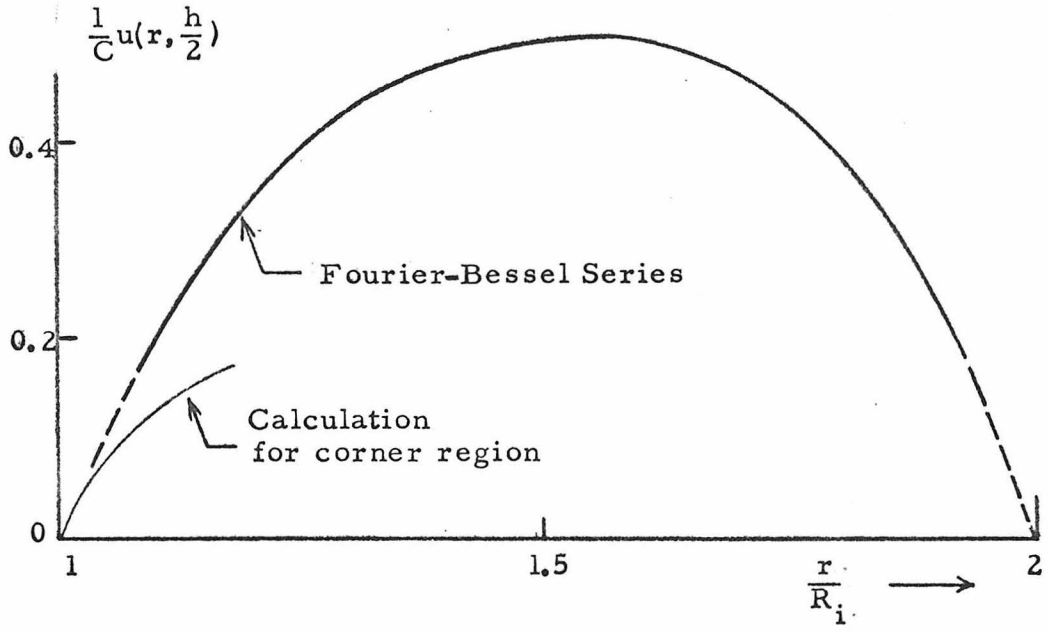

Figure 7

Plot of the velocity along the upper boundary of a cell as given by the Euler solution. Square cell, $Ru/R_i = 2$.